

**FINITE ELEMENT ANALYSIS OF
POLYDIMETHYLSILOXANE (PDMS) STRAIN
SENSOR FOR THE SPINAL FUSION
MONITORING**

By:

NG HAN WEI

(Matric no.: 137853)

Supervisor:

Dr. Inzarulfaisham Bin Abd Rahim

July 2021

This dissertation is submitted to
Universiti Sains Malaysia
As partial fulfillment of the requirement to graduate with honors degree in
BACHELOR OF ENGINEERING (MECHANICAL ENGINEERING)



School of Mechanical Engineering
Engineering Campus
Universiti Sains Malaysia

DECLARATION

This work has not been accepted in substance for any degree and is not being concurrently submitted in candidature for any degree.

Signed.......... (NG HAN WEI)

Date.....12/7/2021.....

Statement 1: This journal is the result of my own investigation, except where otherwise stated. Other sources are acknowledged by giving explicit references. Bibliography/references are appended.

Signed.......... (NG HAN WEI)

Date.....12/7/2021.....

Statement 2: I hereby give consent for my journal, if accepted, to be available for photocopying and for interlibrary loan, and for the title and summary to be made available outside organizations.

Signed.......... (NG HAN WEI)

Date.....12/7/2021.....

ACKNOWLEDGEMENT

I would like to offer my special thanks to University of Science, Malaysia (USM), Engineering Campus to give me chance to conduct a Final Year Project. Then, I would like to thanks my project supervisor, Dr. Inzarulfaisham Bin Abd Rahim who always gives me suggestive advice to complete my project especially from aspect of the technical support. Besides, I wish to acknowledge the help provided by Muhammad Irsyad Bin Abdul Mokti by giving advice to complete the project. A very special gratitude goes out School of Mechanical Engineering to provide the Turnitin plagiarism checking service to ensure the similarity percentage of thesis follows acceptance criteria. Moreover, I would like to express my very great appreciation to USM engineering Library that provides the thesis formatting webinar that hosted by Madam Noor Anisah Khadiri. Last but not the least, I would like to thanks Ts. Dr. Muhammad Hafiz Hassan for held the FYP thesis writing webinar.

TABLE OF CONTENTS

DECLARATION	ii
ACKNOWLEDGEMENT	iii
TABLE OF CONTENTS	iv
LIST OF TABLES	vii
LIST OF FIGURES	viii
LIST OF SYMBOLS	xi
LIST OF ABBREVIATIONS	xiii
List of appendix.....	xiv
ABSTRAK.....	xv
ABSTRACT	xvii
CHAPTER 1 INTRODUCTION.....	1
1.1 Overview.....	1
1.2 Spinal fusion	1
1.2.1 Spinal deformities	1
1.2.2 Spinal weakness or instability.....	2
1.2.3 Herniated disk	2
1.2.4 General Spinal Fusion Procedure (<i>Spinal Fusion - Mayo Clinic, n.d.</i>).....	3
1.3 Application of capacitive based sensor in spinal fusion monitoring	3
1.4 Project Background	4
1.5 Problem Statement	5
1.6 Research objectives	6
1.7 Scope of Work.....	6
1.8 Thesis outline	7

CHAPTER 2	LITERATURE REVIEW	8
2.1	Overview.....	8
2.2	Capacitive Sensor and Sensing Mechanism	8
2.2.1	Dielectric material.....	8
2.2.2	Electrode gap	9
2.2.3	Overlapping Area.....	12
2.3	Capacitive Strain Sensor.....	13
2.4	PDMS Based Sensor.....	15
2.4.1	Application of the PDMS in Sensor.....	15
2.4.2	Mechanisms and techniques used for PDMS based capacitive sensor.....	17
2.5	Finite Element Analysis.....	18
2.6	Summary.....	19
CHAPTER 3	METHODOLOGY.....	20
3.1	Overview.....	20
3.2	Design Detail of Sensor	20
3.3	Simulation Process	21
3.3.1	Stress Analysis.....	21
3.3.1(a)	Stress Analysis: To determine the load generating 1000 $\mu\epsilon$	22
3.3.1(b)	Stress Analysis: Create the deformed geometry of 2D sensor model	23
3.3.2	Electrostatic Analysis: To obtain the capacitance output.....	24
3.4	Working Mechanism of the Sensor	25
3.5	Summary.....	29
CHAPTER 4	RESULT AND DISCUSSION	30
4.1	Overview.....	30
4.2	Wrong Deflection Effect of the Cantilever Beam.....	30

4.3	Thickness of the anchor	31
4.3.1	Comparison between the simulated capacitance output to the calculated capacitance value.....	31
4.3.2	Comparison between the simulated capacitance output to the design model (Mokti et al., 2011).....	35
4.4	Anchor Length	35
4.4.1	Comparison between the simulated capacitance output to the calculated capacitance value.....	36
4.4.2	Comparison between the simulated capacitance output to the design model (Mokti et al., 2011).....	39
4.5	Dielectric Coverage	39
4.5.1	Comparison between the simulated and calculated result.....	40
4.5.2	Comparison between the simulated capacitance output to the design model (Mokti et al., 2011).....	42
4.6	Simulation Study	43
4.7	Summary.....	45
CHAPTER 5 CONCLUSION AND FUTURE RECOMMENDATIONS		46
5.1	Conclusion	46
5.2	Recommendation for Future Works	47
LIST OF PUBLICATIONS		

LIST OF TABLES

	Page
Table 3-1	Material Properties of the Parts 21
Table 3-2	Table of the displacement and strain 23
Table 3-3	Dielectric constant of the material 24
Table 3-4	Value of variables for calculation 28
Table 4-1	Capacitance output of Simulated and Calculated Result 33
Table 4-2	Percentage different of 1.5 μ m, 3 μ m and 5 μ m Electrode Gap 34
Table 4-3	Comparison Result for 1.5 μ m, 3 μ m and 5 μ m Electrode Gap 35
Table 4-4	Capacitance output of Simulated and Calculated Result for 0.5mm, 1mm and 1.5 mm 37
Table 4-5	Percentage different of the Anchor Length of 0.5mm, 1mm and 1.5mm 38
Table 4-6	Comparison Result for 0.5mm, 1.0mm and 1.5mm Anchor Length 39
Table 4-7	Capacitance output of Simulated and Calculated Result for 100%, 66% and 33% dielectric coverage 41
Table 4-8	Percentage different of the Anchor Length of 0.5mm, 1mm and 1.5mm 42
Table 4-9	Comparison Result for 0.5mm, 1.0mm and 1.5mm Anchor Length 42

LIST OF FIGURES

	Page
Figure 1-1 The SFMI implant attached to a spinal fusion rod. (Lin et al., 2007)	4
Figure 2-1 Schematic of the loading–unloading cycle for the GO foam pressure sensor (Wan et al., 2017)	9
Figure 2-2 Plating Structure of electro-conductive fabric (Min et al., 2014).....	10
Figure 2-3 abdominal circumference changes in every respiration: (a) Inhalation process. (b) Exhalation process. (Min et al., 2014).....	10
Figure 2-4 Abdominal circumference changes in every respiration (c) The distance between plates is varied by respiration. In inhalation, outward force is generated and it makes the distance between plates shorter and the area larger. (Min et al., 2014)	10
Figure 2-5 Structure of the fabricated sensor (Vu & Kim, 2020)	11
Figure 2-6 Working mechanism of the sensor before and after loading pressure(Vu & Kim, 2020).....	11
Figure 2-7 Schematic of the proposed capacitive pressure sensor: (a) top view of the sensor’s structure, (b) cross-section of the sensor’s structure (Z. Liu et al., 2019).....	12
Figure 2-8 Schematic flow charts of two types of the stretchable strain fabrication process; (c) capacitive sensor fabrication (Dong et al., 2021).....	13
Figure 2-9 Working principle of capacitive sensor; (a) Initial state; (b) Stretched state. (Dong et al., 2021).....	13
Figure 2-10 Schematic illustration of the working mechanism of a DES: (a) a DE film sandwiched by two flexible electrodes (b) when the DE film is stretched (X. Liu et al., 2021).....	14

Figure 2-11	an illustration of the elevated comb drive or inter-digitized finger capacitive design with two independent anchors. (Aebersold et al., 2006).....	15
Figure 2-12	Structure of PDMS (Kuncová-Kallio & Kallio, 2006)	15
Figure 2-13	Schematic showing the configuration of the GR/PDMS sponge under force (Kou et al., 2019)	16
Figure 2-14	Illustration of the structure of the capacitance micro-sensor (Lei et al., 2012).....	17
Figure 2-15	transparent sensor based on PDMS-embedded conductive fabric (Nag et al., 2018)	18
Figure 2-16	Illustration of the effect of the induced strain on the overall dimensions of the sensor. (Nag et al., 2018)	18
Figure 3-1	Sensor structure and part name.....	20
Figure 3-2	Sensor dimensions (Mokti et al., 2011)	20
Figure 3-3	Assembly of the sensor	22
Figure 3-4	Stress analysis of the Sensor Model	22
Figure 3-5	2D sketching of the sensor	23
Figure 3-6	Meshed model.	24
Figure 3-7	De-formed geometry of the sensor	24
Figure 3-8	Cantilever beam bending schematic diagram (Mokti et al., 2011)...	25
Figure 3-9	Sensor deflection schematic diagram (Mokti et al., 2011)	26
Figure 4-1	Graph of displacement (mm) versus load (Mpa) before changing of beam young modulus	30
Figure 4-2	Graph of displacement (mm) versus load (e+1Mpa) after changing of beam young modulus.....	31
Figure 4-3	Graph of capacitance versus strain of 1.5 μ m anchor gap	32
Figure 4-4	Graph of capacitance versus strain of 3 μ m anchor gap	32
Figure 4-5	Graph of capacitance versus strain of 5 μ m anchor gap	32

Figure 4-6	Sensitivity versus anchor thickness of sensor	34
Figure 4-7	Graph of capacitance versus strain of 0.5mm	36
Figure 4-8	Graph of capacitance versus strain of 1.0 mm	36
Figure 4-9	Graph of capacitance versus strain of 1.5mm	37
Figure 4-10	Sensitivity versus anchor length of sensor	38
Figure 4-11	Graph of capacitance versus strain of 33% Dielectric Coverage	40
Figure 4-12	Graph of capacitance versus strain of 66% dielectric coverage	40
Figure 4-13	Graph of capacitance versus strain of 100% dielectric coverage	40
Figure 4-14	Sensitivity versus dielectric coverage of sensor	41
Figure 4-15	Percentage error versus strain value	43
Figure 4-16	Manual meshed.....	44
Figure 4-17	Automatic meshed	44

LIST OF SYMBOLS

SYMBOL	DESCRIPTION	UNIT
C	Capacitance	pF
ϵ_0	Relative permittivity of free space (8.85×10^{-12})	F.m ⁻¹
ϵ_r	Dielectric constant	-
A	Area of the overlaps electrodes	m ²
D	Electrode gap	m
ϵ	Strain	-
Σ	Normal stress in the member	N.m ⁻²
max σ	The maximum normal stress in the member	N.m ⁻²
M	The resultant internal moment	N.m
M_x	The resultant internal moment along x -axis	N.m
I	The moment of inertia of the cross-sectional area computed about the neutral axis	m ⁴
E	Young's Modulus	N.m ⁻²
ν	Poisson's ratio	-
max c	The farthest point perpendicular to neutral axis	m
θ	Slope	rad
L	Total length of the beam	m
P	Pressure load	N.m ⁻²
V	Deflection in y -axis	m
v_d	Tangent deflection of the top layer of the sensor	m
W	Width of the beam	M

SYMBOL	DESCRIPTION	UNIT
l_0	Distance between $x=0$ to the first point of the sensor	m
l_1	Distance between $x=0$ to the last point of the sensor	m
l_2	Distance between $x=0$ to the last point of the anchor of the sensor	m
l_3	Distance between $x=0$ to the first point of the anchor of the sensor	m
B	Integral constant	-
D	Average electrode gap	m
x_1	First point along the sensor electrode	m
x_2	Second point along the sensor electrode	m
C_T	Total capacitance	pF
C_1	Capacitance of anchor (Pdms)	pF
C_2	Capacitance of air gap	pF
C_3	Multilayer dielectric capacitance	pF
C_{air}	Capacitance of air area	pF
C_{Pdms}	Capacitance of dielectric area	pF
ΔC	Capacitance change between two points of bending	pF
$\Delta \varepsilon$	Strain change between two points of bending	-
A_1	Anchor (Pdms) area	m ²
A_2	Air gap area	m ²
A_{Pdms}	Dielectric area	m ²
d_{air}	Initial gap (dielectric area)	m
d_{Pdms}	Dielectric thickness	m
D_{air}	The average gap of the electrodes opening during bending at the air area	m
D_{Pdms}	The average gap of the electrodes opening during bending at the dielectric area	m

LIST OF ABBREVIATIONS

Abbreviations	Description
PDMS	Polydimethylsiloxane
FEA	Finite Element Analysis
3D	Three Dimension
2D	Two Dimension
MRI	Magnetic resonance image
CT Scan	Computed tomography scan

LIST OF APPENDIX

Appendix List	Description
Appendix-A	STRESS ANALYSIS TO DETERMINE THE STRAIN VALUE
Appendix-B	RESULT OF THE STRAIN VALUE BY CHANGING THE YOUNG MODULUS OF THE TEST BEAM FROM $1.69E+14$ TO $1.69E+15$
Appendix-C	ATTACHMENT TO SHOW THE MESH SIZE LIMITATION OF THE SOFTWARE

ABSTRAK

Dalam projek ini, Simulasi Elemen Terhingga yang berkaitan PDMS sensor regangan berkapasitif telah dilakukan untuk memerhatikan prestasi sensor dalam pemantauan peleburan tulang belakang dari aspek sensitiviti sensor dan kapasitansi nominal. Reka bentuk dan dimensi sensor berasal daripada reka bentuk sensor (Mokti et al., 2011). Dalam projek ini, bahan dielektrik ditukar kepada Polydimethylsiloxane (PDMS) untuk memerhatikan perubahan dari segi prestasi sensor. Hasil simulasi akan dibandingkan dengan hasil yang terdapat dalam reka bentuk (Mokti et al., 2011) dan disahkan oleh kaedah pengiraan. Kaedah gambar radiografi tidak dapat menggambarkan perkembangan proses peleburan tulang belakang secara tepat dan efektif. Oleh itu, kaedah alternatif sangat diinginkan. Sensor regangan berkapasitif dikehendaki kerana ia hanya memerlukan penggunaan kuasa yang rendah. Hal ini kerana, arus terus (AT) tidak akan mengalir secara melalui elemen sensor. Bahan dielektrik yang digunakan dalam model sensor ini adalah PDMS yang sesuai ditanam di tulang belakang manusia kerana sifat materialnya yang tidak serasi, tidak beraktif secara kimia dan tidak beracun. Selain itu, PDMS selalu digunakan untuk membuat sensor kerana ia mempunyai Modulus Elastisitas yang lebih rendah. Ini telah menunjukkan kebaikan PDMS untuk mengurangkan tahap kerumitan dalam proses fabrikasi. QuickField Student 6.5 telah digunakan sebagai perisian untuk melakukan analisis elemen terhingga. Dalam hal yang demikian, QuickField Student 6.5 akan mensimulasikan output kapasitansi sensor. Terdapat tiga parameter reka bentuk dalam projek ini iaitu panjang jangkar, ketebalan jangkar dan liputan dielektrik. Dari perspektif hasil simulasi yang didapatkan, ia diperhatikan bahawa sensitiviti sensor akan meningkat ketika ketebalan jangkar dan panjang jangkar akan ditingkatkan.

Liputan dielektrik akan menghasilkan output kapasitansi dan sensitiviti yang tertinggi di antara tiga parameter. Nilai sensitiviti sensor dalam hasil simulasi untuk perubahan liputan dielektrik 100%, 66% dan 33% adalah $0.1927\text{pF}/\mu\epsilon$, $0.1607\text{pF}/\mu\epsilon$ dan $0.1282\text{pF}/\mu\epsilon$ masing-masing. Jika berbanding dengan hasil simulasi yang didapati dalam kajian ini, nilai sensitivity yang terdapat dalam (Mokti et al., 2011) model reka bentuk adalah lebih besar iaitu bernilai $0.2513\text{ pF}/\mu\epsilon$, $0.1906\text{ pF}/\mu\epsilon$ dan $0.122\text{ pF}/\mu\epsilon$ daripada liputan dielektrik 100%, 66% dan 33% masing-masing. Selain

itu, kapasiti nominal untuk tiga liputan dielektrik yang dimanipulasi pada sensor didapati lebih tinggi dalam (Mokti et al., 2011) model reka bentuk. Ini mungkin disebabkan oleh pemalar dielektrik PDMS adalah lebih kecil daripada silikon dioksida.

ABSTRACT

In this project, Finite Element Simulation of PDMS capacitive bending strain sensor is conducted in order to observe the sensor performance in application of spinal fusion monitoring from the aspect of the sensitivity and nominal capacitance. The sensor design and dimension is originated from the sensor design (Mokti et al., 2011). In this project, dielectric material is manipulated to Polydimethylsiloxane (PDMS) to observe the change in sensor performance output. The simulated result is then compared to the result of design (Mokti et al., 2011) and verified by the calculation result. The current methods using a radiographic image do not reflect the fused spine progression accurately and therefore alternative methods are highly desired. Capacitive strain sensor is desired due to its low power consumption. This is because there is no DC current flow through the sensor element. Dielectric material used in this sensor model is PDMS that is suitable to be implanted in the human spinal bone because of its material properties of biocompatible, chemically inert and non-toxic. Besides, it is always been utilised to fabricate sensor due to its lower young modulus. This is a benefit to reduce the complexity level of fabrication process. QuickField Student 6.5 is the Finite Element Analysis (FEA) software used in this project to simulate the sensor capacitance output. There are three design parameters at which are the anchor length, anchor thickness and dielectric coverage in this project. Regarding to the simulated result, it was observed that the sensitivity is increased when anchor thickness and anchor length are increased. Among the three parameters, the dielectric coverage will result in highest capacitance output and sensitivity. The value of the sensitivity in the simulated result for 100%, 66% and 33% dielectric coverage are $0.1927\text{pF}/\mu\epsilon$, $0.1607\text{pF}/\mu\epsilon$ and $0.1282\text{pF}/\mu\epsilon$ respectively at which are smaller than that in (Mokti et al., 2011) design model at which are $0.2513\text{ pF}/\mu\epsilon$, $0.1906\text{ pF}/\mu\epsilon$ and $0.122\text{ pF}/\mu\epsilon$ respectively. Besides, the nominal capacitance of the three manipulated dielectric coverage in sensor is found higher in (Mokti et al., 2011) design model. This probably due to the dielectric constant of PDMS is slightly smaller than silicon dioxide.

CHAPTER 1

INTRODUCTION

1.1 Overview

This chapter will begin with the basic concept of spinal fusion instrumentation and followed by project background, research objective, problem statement and thesis layout. Project background gives brief idea to show the project potential and improvement on the future sensing technology in spinal fusion monitoring process. Research objective shows the main goal to be achieved in the end of the study while the problem statement describes the current condition of the project that tends to be improved. Lastly the thesis layout will list down the summary of each chapter.

1.2 Spinal fusion

Spinal fusion is a surgical procedure at which is carried out to fuse spinal bone. The position of the spinal bone is fixed by using screw and metal plates to make sure the fused bone heal into a single new bone unit. Spinal fusion is one of the surgery options used to treat the deformities of the spine, spinal instability and herniated disk. (*Spinal Fusion - Mayo Clinic*, n.d)

1.2.1 Spinal deformities

Spinal deformity can be defined as disease that causes the abnormal curvature of spine. In this case, the spine has two gentle front-to-back curvature structures. Sagittal imbalance is an example of the spinal deformity that causes front-to-back imbalance in the spine. There are two types of the sagittal imbalance which are flat-back syndrome and kyphosis. When the lumbar spine loses normal lordosis, the condition can be explained by flat-back syndrome. In this case, the outward curve of the thoracic spine is therefore the only curve, and the centre of gravity juts too far forward. Kyphosis is another type of sagittal imbalance. In this case, the normal kyphosis of the thoracic spine is raised until causing the back appears hunched.

Scoliosis is another form of deformity found in the spine that able to be observed from the back. (*Spinal Deformities*, n.d.) Scoliosis is defined as high complexity three-dimensional (3D) spinal deformity of unknown aetiology. Scoliosis

might bring a considerable impact on morphology and movement of the human body. In this case, the patient that diagnosed with scoliosis will have lateral curvature of the spine greater than 10°. This kind of deformity that is comprised changes at lateral shift in coronal plane particularly. (Delpierre, 2020) In this case, spinal fusion surgery aims to correct the spinal curve, particularly in coronal and sagittal planes.

1.2.2 Spinal weakness or instability

Patient with spinal instability will always feel low back pain. This is a common disease that resulting from degeneration of the intervertebral joint. In this case, it losses of stiffness and it might cause the joint cannot perform sufficient strength to the spine structure. Besides, spinal instability will weaken the muscle that supports the spine structure. Electromyography and ultrasound device are commonly used in detect the abnormality of the spine structure. Ultrasound may show a wasting of deep spinal muscles and electromyography (EMG) is able to detect muscle change in spine.

In order to restore stability and make the spine structure stronger, spinal fusion is needed for patients who are not prefer to continue with conservative treatment.(Dang et al., 2020)

1.2.3 Herniated disk

From the aspect of the anatomy, the cervical spine is constructed by seven vertebral bodies and intervertebral discs anchored to the bodies through endplate areas. In this case, the disc is composed of nucleus pulposus and annulus fibrosus. Herniated disk is occurred when the inner nucleus pulposus protrudes through the annulus fibrosus.

Herniation of the disc in the cervical area may occur suddenly from a traumatic incident or overtime by degenerative and mechanical changes. The most common level of cervical disc herniation in the cervical (C) 5–6 and 6–7 vertebrae compressed C6 and C7 roots. (Tobing & Aprianto, 2020).A herniated disk is commonly found at the lower back and it is called as a bulging, protruding, or ruptured disk. One of the symptoms is having low back pain and leg pain caused by a herniated disk. To treat the case of herniated disk, spinal fusion functions to stabilize the spine after removal of damage disk. (*Herniated Disk in the Lower Back - OrthoInfo - AAOS*, n.d.)

1.2.4 General Spinal Fusion Procedure (*Spinal Fusion - Mayo Clinic, n.d.*)

Spinal fusion procedure includes the incision, bone graft preparation and fusion process. In incision process, in order to gain access to the vertebrae being fused, surgeon makes an incision in one of three locations at which the area located around neck or back directly over along the spine, on either side of spine, or in abdomen or throat. This is to ensure that surgeon can access the spine from the front.

Then, the procedure will proceed with bone graft preparation. The bone grafts that actually fuse two vertebrae together may come from a bone bank or from patient own body, usually from pelvis. The surgeon makes an incision above the pelvic bone, removes a small portion of it and then closes the incision when the patient own bone is utilized in bone graft preparation.

The last step is the fusion stage. In order to fuse the vertebrae together permanently, surgeon places the bone graft material between the vertebrae. Metal plates, screws or rods may hold vertebrae together while the bone graft heals.

1.3 Implantation of capacitive based sensor in spinal fusion monitoring

According to (Kanayama et al., 1997), a study relates to the posterolateral fusion was conducted in order to observe the bone fusion mass properties and shared load characteristic that exhibited by implanted rod to the 24 sheep within a time period. From study conducted by (Kanayama et al., 1997), the load shared by the rod decreasing as the fusion mass increases and the bone became stiffer. When the bone fusion is occurred, the implanted rod will generate the significant amount of bending stress if compare to axial stress. Therefore, the bending stress generated by the implanted rod can be utilized as data to monitoring the spinal fusion progression.

(Lin et al., 2007) proposed capacitive based bending strain sensor with cantilever beam structure in order to monitor the spinal fusion progression. The sensor is required to detect strain value from 0 to $1000\mu\epsilon$. In this case, sensor should exhibit its high sensitivity in order to detect the smallest change in the strain. Size limitation of 2mm in width and 10mm in length of the sensor is suggested. Length of sensor including the sensor housing is suggested at about 12.5mm at which is half of the distance between two vertebrae is about 25.4 mm in the lumber region.

Figure 1-1 shows that the sensor housing is located between two Pedical screws. Flat area (2mm x 10mm) is created by cutting the 1mm down at curve surface of the implanted rod. Then, the sensor is mounted on the flat surface of the implanted rod.

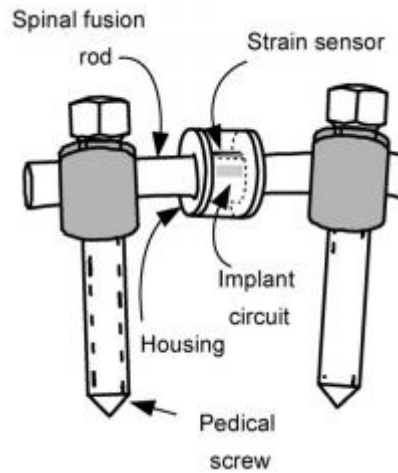


Figure 1-1 The SFMI implant attached to a spinal fusion rod. (Lin et al., 2007)

1.4 Project Background

In this project, Finite Element Analysis software used is the QuickField Student 6.5. Capacitance output from the PDMS bending strain sensor is simulated since it will be a significant factor to determine the sensing performance in process of spinal fusion monitoring. Spinal fusion is a surgical procedure used to correct problems with the bones in the spine (vertebrae), at which including herniated disk, spinal deformities and spinal instability. It is necessary to have a monitoring process on the spinal vertebrae fusion progression in the recovery period of the surgery. An implantable PDMS capacitive bending strain sensor is proposed in this project due to few reasons.

Firstly, bending strain is measurable on the spinal fusion fixture; it may be either a metal plate or rod. In this case, bending strain for the implanted sensor will be decreased when the grafted bone is fused. This may be due to the load transfer to the fused bone. Therefore, amount of strain is an indicator of the load applied to the metal plate during the bone fusion. Sensor monitoring system is considered more convenient and effective if compared to the standard method such as x-ray images, computed tomography scan (CT-Scan) or magnetic resonance image (MRI). This is because of these available standard methods will not interpret the radiograph image

accurately and it is not effective to detect the presence of the fusion area among bones. Besides, by using radiography image, higher cost is charged. Then, these standard methods may expose the patients to significant radiation, and, more importantly, it does not provide a real time data of the spinal fusion progression.

Polydimethylsiloxane (PDMS) is chosen as the sensor dielectric material in this project. This is due to PDMS's material properties such as optically clear, chemically inert and non-toxic. Besides, PDMS gives good elasticity which serves well for instance in applications involving bending or twisting. This is important for sensing application that involves the strain measurement and it may be used to fabricate the sensor for spinal fusion monitoring. Apart from this, PDMS is biocompatibility; this means that it does not produce a toxic or immunological response when exposed to the body or bodily fluids. Therefore, it is suitable for material sensor implantation in human spine.

While doing the Finite Element analysis, it is necessary to consider the sensor structure and capacitive sensing mechanism. With applying load, the change in sensor structure in term of the deflection will affect the average gap in between two electrodes, followed by affecting the capacitance drop and sensitivity of the sensor. Besides, the manipulation variable such as dielectric constant, area of overlap between the electrodes and electrode gaps are used to determine capacitance response according to the sensor mechanism design.

1.5 Problem Statement

Spinal fusion monitoring using standard method such as the X-ray, MRI and CT- Scan shows limitation in displaying the real time data. Besides, the standard method is costly. So, sensing monitoring system is suggested. In this case, capacitive based sensor shows its strength due to its low power consumption.

Among the current available design for the capacitive based sensor in application of the spinal fusion monitoring, sensor structure of cantilever beam is proposed for measuring the bending strain. Cantilever beam structure of sensor able to measure the bending strain when it is attached to the spinal rod that encounter bending. PDMS exhibits its potential as dielectric material in monitoring sensor since it has low young modulus at which will make the sensor easily to be strained.

Besides, it shows high biocompatibility that will not produce the toxic when it faced to the bodily fluid.

Comparison is made to the sensor model of (Mokti et al., 2011) with replacing the dielectric material to PDMS. This is important to simulate sensing performance when PDMS is used as dielectric material at which is affected by manipulation of the parameters such as anchor length, anchor thickness and dielectric coverage to avoid unnecessary fabrication. The comparison is made between result of these 2 sensor models from aspect of the sensor sensitivity and the nominal capacitance. High sensitivity of the sensor is important to detect the small change in strain. Sensitivity is the important design parameter of any sensor, which defines as the amount of output quantity changes with respect to changes presented in the input quantity while the high nominal capacitance is important to prevent the sensor from losing its real time monitoring data. Therefore, it is necessary to simulate the sensor performance which is sensitivity and nominal capacitance of the PDMS strain sensor model.

1.6 Research objectives

1. To simulate the sensor sensitivity and nominal capacitance of the PDMS based capacitive bending strain sensor.
2. To verify the simulated result of sensor sensitivity and nominal capacitance by comparing it to the theoretical value.
3. To compare sensor performance between simulated models sensor to the other sensor model that using different dielectric material.

1.7 Scope of Work

The project aimed to simulate the sensitivity of the implantable PDMS capacitive strain sensor for spinal fusion progression monitoring. The process starts with study on the literature review regarding to the research topic and related sensors structure with respective the sensing mechanism. After that, the sensor design is selected by manipulating the dielectric material to the PDMS. Then, finite element analysis is conducted with verification step by comparing to calculated

theoretical value. Finally, the simulated result is compared with the same designed sensor with different dielectric material.

1.8 Thesis outline

Five chapters are found in this thesis. Chapter 1 introduced about the basic concept of the spinal fusion. Besides, the project background is explained in this chapter to deliver the main idea and objectives in this project. Problem statement describes the current condition of the project that tends to be improved.

Chapter 2 is a literature review to shows the related content from the reference sources such as journal, science article and thesis. Sensing mechanism of capacitive sensor, capacitive strain sensor and PDMS based sensor are the common topic that will be discussed in this chapter.

Chapter 3 presents the methodology to perform FEA software simulation and the calculation step to evaluate and verifying the performance of sensor model. Design detail is explained and the analytic parameter such as the anchor length and anchor thickness, and the dielectric coverage are manipulated in simulation process.

Chapter4 shows the simulated and calculated result of the sensor model. The simulated result is compared to the calculated result to get the percentage different to find the similarity between these two types of result to complete the result verification. Comparison between the simulated result and design sensor result (Mokti et al., 2011) from the aspect of the capacitance output and sensitivity.

Chapter 5 presents a conclusion and the future work is suggested to improve the project result and its application in real life.

CHAPTER 2

LITERATURE REVIEW

2.1 Overview

Chapter 2 is a literature review regarding to this project, the reference source are taken form the journal, science article and some thesis. The list of the topic that is review through this chapter including the sensing mechanism of capacitive sensor, capacitive strain sensor and PDMS based sensor.

2.2 Capacitive Sensor and Sensing Mechanism

Capacitive sensor is constructed based on sandwich-like structure that built up by 2 electrodes and middle layers of dielectric material. Working mechanism of capacitive sensor relates to the theory of deformation of a capacitor. (Li et al., 2021) Deformation of the capacitor sensor structure will cause the change in capacitance output. Equation of the capacitance given as below:

$$C = \frac{\epsilon_0 \epsilon_r A}{d}$$

Where

ϵ_0 = Relative permittivity of free space (8.85x10 F.m)

ϵ_r = Dielectric constant

A = Area of overlap between the electrodes

d = Gap between the electrodes

According to the equation above, overlapping area between electrodes, dielectric constant and gap between electrodes are the manipulating variables for the capacitance output in capacitive based sensor. The manipulating variables are discussed in detail in following sections.

2.2.1 Dielectric material

Dielectric material is one of the important factors to improving the capacitance output. Ultra-sensitive Graphene Oxide(GO)-based capacitive pressure sensor that is developed by (Wan et al., 2017) shows the effect of the dielectric material on the

capacitance output. In this design, the electrode of this sensor is made up of the graphene. Then, Graphene Oxide (GO) is chosen to be the dielectric material for the sensor. This is because of its material properties that shows the increment of dielectric when the electrode gap is reduced when it is pressed. The sensing mechanism of the sensor is illustrating as the figure 2-1.

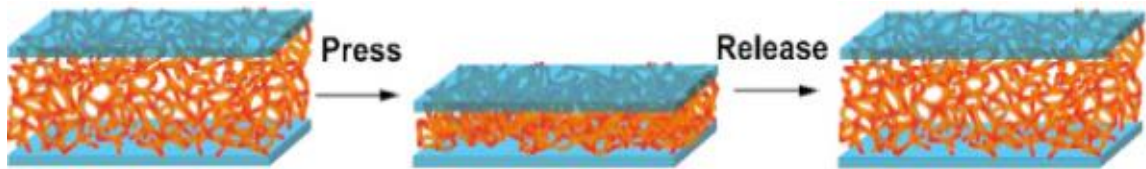


Figure 2-1 Schematic of the loading–unloading cycle for the GO foam pressure sensor (Wan et al., 2017)

From the illustration, GO foam is located in between two graphene electrodes. In the loading process, it is compressed when the external pressure pressing on the surface of the top electrode and the capacitance in GO foam is increased due to the distance between the two graphene electrodes is decreased. In this case, air void in GO foam is compressed and causes air displacement. Air has a lower dielectric constant at which is 1.0 while GO foam will have the dielectric constant at about 10. In this condition, the effective dielectric constant is increased by adding up dielectric constant from air and GO. In short, the decreasing of electrode gap and increasing of effective dielectric constant are the reasons to cause the higher capacitance output and sensor sensitivity.

This sensor can determine the subtle pressure in a fast response time. In this case, subtle pressure of 0.24 Pa is detected within a short time at which is about 100ms. Due to this, It is suitable to be applied in the many fields, for an example, it can be used for the health monitoring process to obtain the real time data to ensure the normal recovery progression rate of the patient.

2.2.2 Electrode gap

A Textile Capacitive Respiration Sensor (TCRS) was developed by (Min et al., 2014) for monitoring the human respiration system. Nickel (Ni) and copper (Cu) are the metals involved to stack with polyester fabric in arrangement of Ni-Cu-Ni to function as an electrode layer. Then, the 100 % polyester is stacked with the conductive electrode layer to build the sensor structure as shown as Figure 2-2 below:



Figure 2-2 Plating Structure of electro-conductive fabric (Min et al., 2014)

TCRS is applied to monitor the human respiration process. In the breathing process, the chest muscle is contracted and the abdominal diameter will be increased to produce the force and this will be detected by TCRS. This condition is illustrated as Figure 2-3 below.

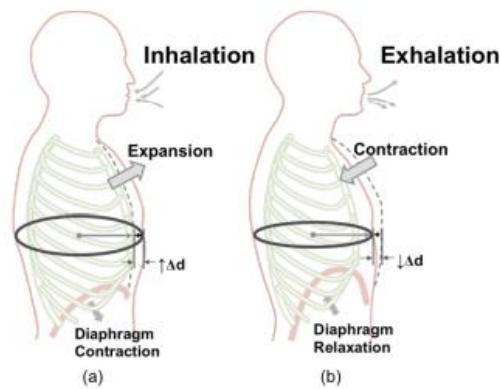


Figure 2-3 abdominal circumference changes in every respiration: (a) Inhalation process. (b) Exhalation process. (Min et al., 2014)

TCRS can detect and measure the force that is generated from the change in capacitance value as responding to the change in gap between two textiles plates. This process is illustrated as figure 2-4 below.

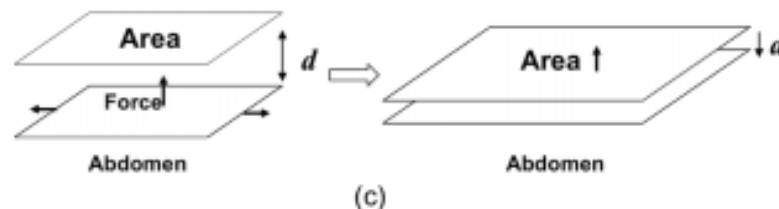


Figure 2-4 Abdominal circumference changes in every respiration (c) The distance between plates is varied by respiration. In inhalation, outward force is generated and it makes the distance between plates shorter and the area larger. (Min et al., 2014)

Another example of sensor that perform capacitive sensing mechanism (Vu & Kim, 2020) based on the change in electrode gap is the capacitive pressure sensor. It is applied to full-range human motion monitoring. The sensor structure is formed by layers of electrode (SWCNT/Silver paste), PET/SP fabric layer and Capsulation/Pet fibre layer as shown as Figure 2-5 below.

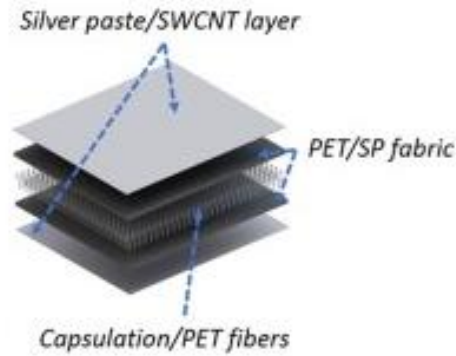


Figure 2-5 Structure of the fabricated sensor (Vu & Kim, 2020)

From the aspect of working principle of the capacitive pressure sensor, the capacitance output is changed according to the change in the electrode gap (Figure 2-6). When the fabric layer (PET/SP fabric) that locates in between two electrodes is applied with pressure load, it will be deformed and causes the electrode gap decreased. As a result, the capacitance output and sensitivity will be increased. Once the pressure load is removed, the deformed fabric layer will return to its original shape. The nominal capacitance is gained in this state.

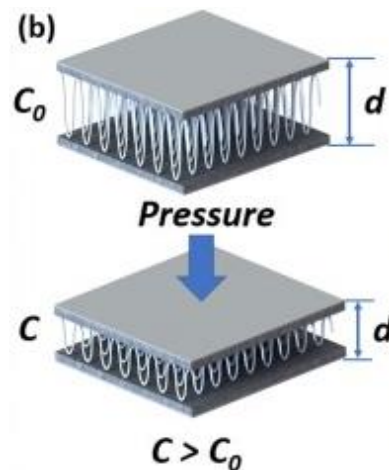


Figure 2-6 Working mechanism of the sensor before and after loading pressure (Vu & Kim, 2020)

2.2.3 Overlapping Area

A capacitive pressure sensor based on non-coplanar comb electrodes is proposed by (Z. Liu et al., 2019) to solve the problem of the nonlinearity that happen in traditional bossed diaphragm capacitive pressure sensors. Figure 2-7 shows the structure of the sensor that composed of three layers of Silicon of Insulator (SOI) that device layer SOI is the first layer, then is followed by oxide layer SOI and handler layer SOI.

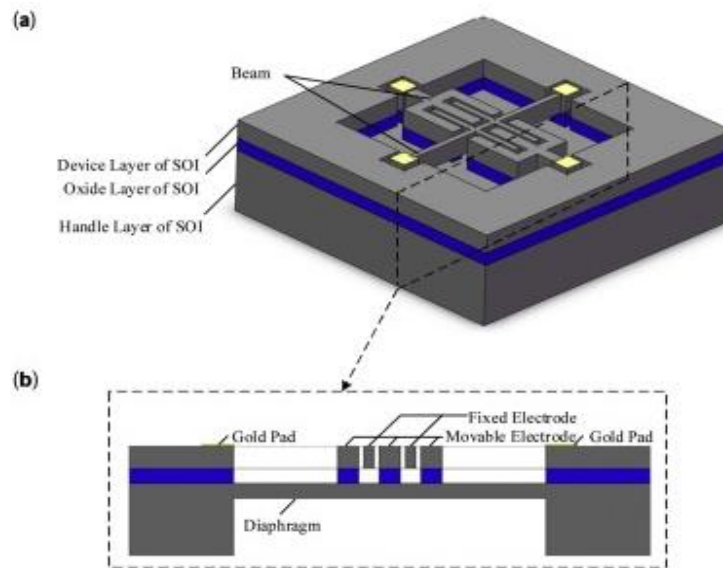


Figure 2-7 Schematic of the proposed capacitive pressure sensor: (a) top view of the sensor's structure, (b) cross-section of the sensor's structure (Z. Liu et al., 2019)

Comb electrode is located in the device layer SOI. In this case, the movable comb electrodes are arranged in crosswise with the fixed comb electrodes. The oxide layer is located at the connection between the fixed comb electrodes and the diaphragm.

The sensing mechanism begins when the pressure load is applied to the diaphragm. Then, the diaphragm will deflect to cause the displacement of movable comb electrodes. Overlap areas between the movable comb electrodes and the fixed comb electrodes is varied and results in the change in sensor capacitance output.

Change in capacitance output indicates that the detected pressure is changed. Sensitivity of the sensor can be improved by connecting the movable comb electrodes to the high-sensitivity area of the diaphragm. This is to ensure the effectiveness to cause the deflection in movable comb electrodes and to generate the huge changes in capacitance drop due to the increasing overlapping area between electrodes.

2.3 Capacitive Strain Sensor

One of the examples of capacitive strain sensor is applied for the wearable application (Dong et al., 2021). The sensor structure is consisted of five layers and shown in stacked arrangement. First layer is first insulation layer then followed by the first electrode layer, the dielectric layer, the second electrode and the second insulation layer. Material of the insulation layers and the dielectric layer is the 3M 4905. Then, the material of the electrodes is made up of the copper.

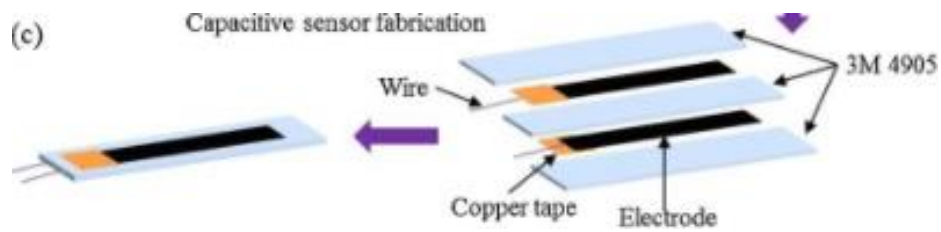


Figure 2-8 Schematic flow charts of two types of the stretchable strain fabrication process; (c) capacitive sensor fabrication (Dong et al., 2021).

Working principle of the capacitive sensor is shown as Figure 2-9 and it is based on the change in capacitance output that yielded from the two copper electrodes when the sensor is applied with tensile strain. In the stretched state, the tensile strain is applied, the sensor length, L is increased while the sensor width, W and thickness, D is decreased. According to the capacitance equation shown below, the capacitance will be increased when the more tensile strain is applied to the sensor.

$$C = \frac{\epsilon_0 \epsilon_r LW}{D}$$

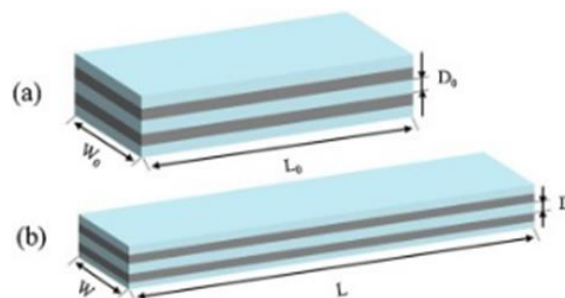


Figure 2-9 Working principle of capacitive sensor; (a) Initial state; (b) Stretched state. (Dong et al., 2021).

The sensitivity of the capacitive strain sensor is influenced by its sensing mechanism that relies on deformed geometry shape of sensor. In this design, the sensitivity found for the capacitive sensor is 0.44.

A dielectric elastomer sensor (DES) with high dielectric constant and capacitive strain sensing properties is proposed by (X. Liu et al., 2021). DES has the sandwich like structure is shown in Figure 2-10, the elastomer film is located between two electrodes.

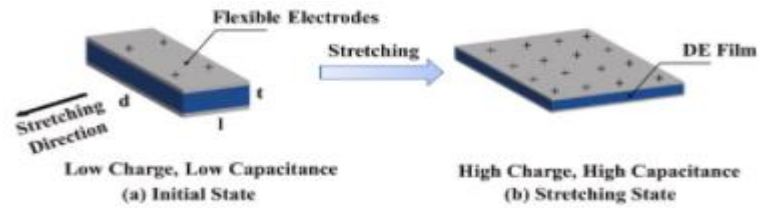


Figure 2-10 Schematic illustration of the working mechanism of a DES: (a) a DE film sandwiched by two flexible electrodes (b) when the DE film is stretched (X. Liu et al., 2021)

From the aspect of the working mechanism, when the sensor is not stretched, the capacitance value is low. After applying the tensile strain, length, l and width, d is increased at DE Film and flexible electrode, the sensor thickness, t is decreased and the capacitance output is increased. The relationship between tensile strain and capacitance output is shown as equation below.

$$C = \frac{\epsilon_0 \epsilon_r l d}{t}$$

A capacitive strain sensor (Aebersold et al., 2006) at which is applied to monitor spinal fusion progression is design with the comb drive sensor structure. This sensor is designed to monitor changes in capacitance that response to change in bending strain of the spinal bone during recovery stage of spinal fusion. The figure below shows the sensor structure:



Figure 2-11 an illustration of the elevated comb drive or inter-digitized finger capacitive design with two independent anchors. (Aebersold et al., 2006)

The sensor is constructed in structure of the inter-digitized finger array at which is made up of highly doped boron silicon wafers. The manufacturing technique called Deep Reactive Ion Etching (DRIE) is used to create desired dimension of sidewalls and spacing between the fingers. Working principle of the sensor may relate to the spacing between the fingers. In this case, by manipulating the spacing between the inter-digitized finger, strain value will be changed. Then, the capacitance output of the sensor will be increased inversely proportional to the strain value.

2.4 PDMS Based Sensor

According to (Kuncová-Kallio & Kallio, 2006), chemical formula of Polydimethylsiloxane (PDMS) is $(C_2H_6OSi)_n$ and it belongs to a group of polymeric organo-silicon compounds called as silicones. PDMS is optically clear, chemically inert, non-toxic, and non-flammable. Its structure is as shown in Figure 2-12 below:

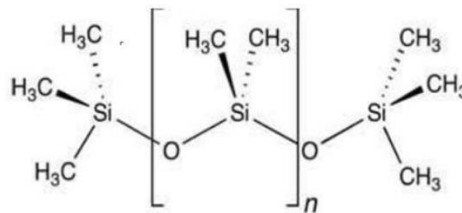


Figure 2-12 Structure of PDMS (Kuncová-Kallio & Kallio, 2006)

PDMS provides good elasticity at which suitable to be applied in the twisting or bending condition. Besides, it may serve well as a dielectric material in sensor and its dielectric constant is from the Taking all these properties such as biocompatibility and conductivity into account, this has been the good choice of material used for biomedical applications.

2.4.1 Application of the PDMS in Sensor

PDMS-based pressure sensor and Wireless wide-range pressure sensor are the sensor examples that currently fabricated using polydimethylsiloxane (PDMS). These sensors have been fabricated utilizing PDMS due to their low Young's modulus and high transparency.

(Hammock et al., 2013) developed a PDMS-based pressure sensor at which is

applied for manufacturing the electronic skins that shows a good sensitivity of 0.55 kPa^{-1} . In this case, this pressure sensor is designed to be more flexible and stretchable in order to mimic the tactile sensing properties of natural skin. (Hammock et al., 2013) reported that this sensor can be fabricated inexpensively due to microstructuring thin films of the PDMS at which functions as a biocompatible elastomer. Besides, the capacitive based pressure sensor is with unprecedented sensitivity and very quick response in such application.

According to (Kou et al., 2019), a wireless flexible pressure sensor is designed for wide range of applications, such as intelligent robots, bionic-electronic skin, and wearable electronic devices. This sensor utilizes a graphene/PDMS (GR/PDMS) sponge as adielectric layer.

By referring to Figure 2-13, the GR/PDMS sponge is positioned between the folded surfaces of a flexible printed circuit with Cu pattern as the antenna and electrode. GR/PDMS sponge is found high performance with high sensitivity, large operating range, rapid response time, low detection limit, good stability, recoverability, and repeatability.

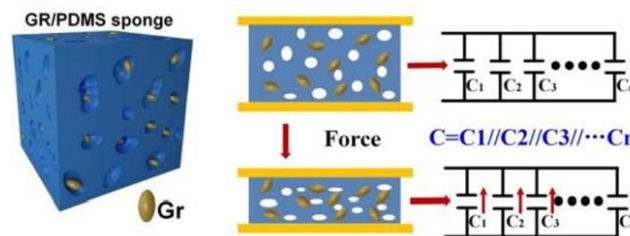


Figure 2-13 Schematic showing the configuration of the GR/PDMS sponge under force (Kou et al., 2019)

The sensing mechanism begins when external pressure load is applied to the sensor and the GR/PDMS sponge will be pressed. This will lead to compression of air-holes. In this condition, GR/PDMS that contains a lot of air-holes will make the sensor more susceptible to deformation when it is under pressure. The gap between Cu electrodes is decreased when the sensor is pressed and causes the total capacitance increased.

2.4.2 Mechanisms and techniques used for PDMS based capacitive sensor

(Lei et al., 2012) have proposed a high sensitive and stable capacitive tactile sensor using PDMS as dielectric layer, which has been successfully applied in wearable electronics. The capacitive pressure sensor consisted of four layers: a lower layer, a dielectric layer, an upper layer, and a bump layer, as illustrated in Figure 2-14.

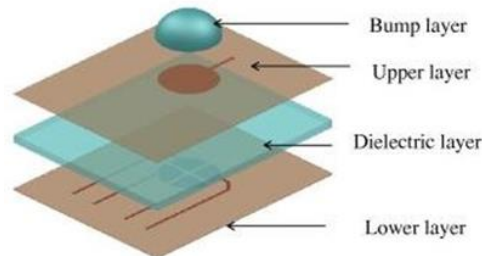


Figure 2-14 Illustration of the structure of the capacitance micro-sensor (Lei et al., 2012)

Flexible printed circuit film is located at both lower layer and upper layer of the sensor structure to function as conductive electrodes. The dielectric layer is made up of PDMS. Sensor structured shows that the dielectric material is sandwiched between two conductive electrodes layer. This sensor able to conduct four independent capacitance measurements by connecting four electrodes to the lower layer and another one electrode is located on the upper layer. The bump layer will create even distribution of the pressure load by providing a point contact between the applied external force load and the sensor electrodes.

The working principle of the sensor is to measure the capacitance change to estimate the applied pressure. In this case, when the bump layer is applied with pressure load, it will evenly distribute the pressure to the layers of material after it, and this will cause the gap between the electrodes is decreased and the capacitance output will be increased. While, the load is removed, only nominal capacitance will be obtained.

According to (Nag et al., 2018), a capacitive strain sensor is designed for wearable sensing applications. The sensor consisted of the inter-digitized fingers that made up of PDMS. This inter-digitized finger is embedded on the conductive fabric as shown as Figure 2-15.

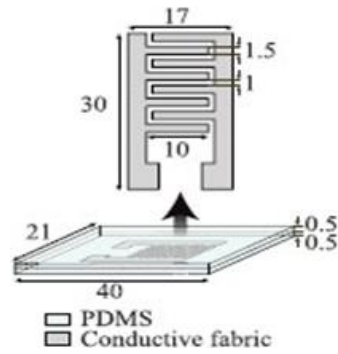


Figure 2-15 transparent sensor based on PDMS-embedded conductive fabric (Nag et al., 2018)

This inter-digitized capacitive strain sensor shows its high flexibility when it is applied with bending strain. In this case, there will be a change in the overall dimensions of the sensor as shown in Figure 2-16.

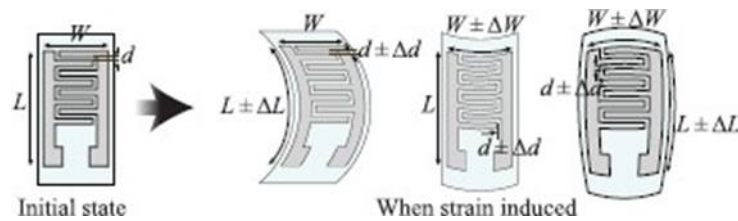


Figure 2-16 Illustration of the effect of the induced strain on the overall dimensions of the sensor. (Nag et al., 2018)

The sensing mechanism begins when the sensor is applied with uniaxial bending strain. In this case, the dimensions of the sensor change, the displacement may happen at the distance between the inter-digitized fingers (d) and the length (L) or width (W) of the sensor. This condition results in a change in capacitance output.

2.5 Finite Element Analysis

Finite element analysis (FEA) software is useful to determine the electrical and mechanical behaviour of the capacitive based sensor. Electrical behaviour that can be studied in the software is the capacitance output, current and voltage. Then, mechanical behaviour of the sensor includes the strain, stress and pressure. COMSOL Multi-physics, CoventorWare, Abaqus are the examples of the FEA software.

COMSOL Multiphysics is software that provides cross-platform finite element analysis, solver and multi-physics simulation. This software provides many simulation features based on a variety of applications including the mechanical, electrical and acoustic based analysis. A capacitive pressure sensor based on non-coplanar comb

electrodes use the COMSOL software to conduct the theoretical analysis and finite element simulation analysis in order to verify the feasibility of the proposed structure. (Z. Liu et al., 2019)

Abaqus is software that performs SIMULIA family of codes. In this case, Abaqus provide multi-physics modelling and simulation. A MEMS capacitive bending strain sensor that is proposed by (Aebersold et al., 2006) is simulated by using ABAQUS/CAE version 6.5 software in order to simulate sensor actuation and capacitance output. Besides, this software is used to study the mechanical behaviour of the sensor structure to avoid the material failure.

CoventorWare able to provide field solvers integrated with pre-processing and post-processing tools. This software has variety of MEMS-specific features. It is preferable to be applied in simulation of MEMS sensor. A capacitive bending strain sensor that proposed by (Mokti et al., 2011) use **CoventorWare™ 2008** to simulate the capacitance output of the sensor.

2.6 Summary

In Chapter 2, literature reviews includes some information and current available sensing mechanism that related to the capacitive based sensor. Three parameters are involved in the sensing mechanism at which are the gap distance, dielectric material and the overlapping area of the electrode. These parameters can be manipulated to obtain the high capacitance output and sensor sensitivity. Besides, various applications of the capacitive based sensors are shown in this chapter. Application for the capacitive pressure sensor includes full-range human motion monitoring and pressure sensing. Then, application of capacitive strain sensor is found in wearable application and spinal fusion monitoring. Textile Capacitive Respiration Sensor (TCRS) is the sensor example that is applied to monitor the human respiratory system by detect the force magnitude change due to the change in the abdominal diameter. In this case, the capacitance value is varied due to change in electrode gap. Another application is related to the dielectric elastomer sensor (DES) that is used to detect the capacitance output that responses to the change in the sensor dimension due to the applied tensile strain.

CHAPTER 3

METHODOLOGY

3.1 Overview

Design parameters of the sensor and finite element simulation process will be discussed in this chapter. Simulated sensor model used in this study is originated from the current available design of capacitive bending strain sensor (Mokti et al., 2011). Simulated sensor model in this project will follow the dimension of the design model (Mokti et al., 2011). Dielectric material will be manipulated from the silicon dioxide to pure PDMS to compare the capacitance output between these 2 models. Then, the simulated result will be evaluated by the FEA software and the simulation output such as the sensor sensitivity and nominal capacitance will be compared to the design model (Mokti et al., 2011) and verified by the calculation result.

3.2 Design Detail of Sensor

Figure 3-1 shows the sensor structure attaching to the test beam while Figure 3-2 shows sensor design detail and sensor dimension.



Figure 3-1 Sensor structure and part name

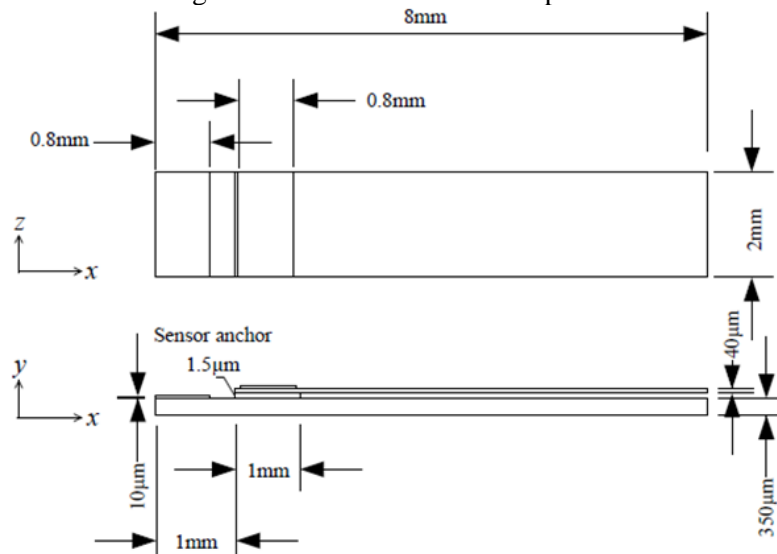


Figure 3-2 Sensor dimensions (Mokti et al., 2011)

This sensor was designed to be implanted to the human spine system. Therefore, it has to follow the sensor size limitation that is determined by distance between the pedicles screws fixed on the lumbar spine. A suggestion was proposed in (Lin et al., 2007) that the implantable sensor should have a limited length at which less than 10mm to fit in the housing of 12.5mm length at which is half of the distance between two vertebrae is about 25.4 mm in the lumber region.

The sensor design detail considers three main parameters to optimize the nominal capacitance and sensor sensitivity at which are the anchor length, anchor thickness and the dielectric coverage percentage. In this study, the dielectric material used is PDMS and result from these three parameters will be compared to the sensor performance of the design model (Mokti et al., 2011).

3.3 Simulation Process

Simulation process includes both stress analysis and electrostatic analysis. Solidwork was chosen to set up the 3D stress analysis of the sensor deflection. The value of distributed load that applied to the sensor was manipulated in order to cause the sensor system strain at $1000\mu\epsilon$. Then 2D stress analysis was continued at the Quickfield Student 6.5. In this case, the sensor model was solved in 2D model to get the deformed sensor geometry before proceed to the electrostatic analysis to simulate the capacitance output.

3.3.1 Stress Analysis

Stress analysis required the material properties such as the young modulus and poison ratio. The table below shows the elastic properties of the material. The material includes the PDMS, aluminum and silicon.

Table 3-1 Material Properties of the Parts

No.	Part	Material	Young Modulus, Pa	Poison Ratio
1	Dielectric Layers and Anchor	PDMS	870000	0.499
2	Electrode	Aluminium	70e+9	0.33
3	Test Beam	Silicon	1.69e+15	0.3

3.3.1(a) Stress Analysis: To determine the load generating $1000\mu\epsilon$

Solid modelling of the sensor was performed in Solidworks. Solid modelling is an important step before the stress analysis. In this case, the dimension of each sensor component should be correct so that simulated result of analysis is accurate. Solid modelling process may include the parts sketching and solid extrusion, and assembly. In this series of process, each of the extruded parts was in correct dimension and they were assembled in proper orientation and position as shown as Figure3-3 below.

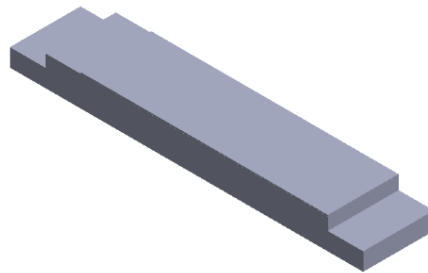


Figure 3-3 Assembly of the sensor

In the stress analysis, each part was applied with their respective material properties. In Solidwork, the material was customized by defining the linear elastic material property including the poison ratio and young modulus. One of the boundary condition is the distributed load at which is applied at negative y-axis to the bottom layer of test beam. Then, one end of the beam is set as a fixed geometry to form the cantilever beam as shown as below:

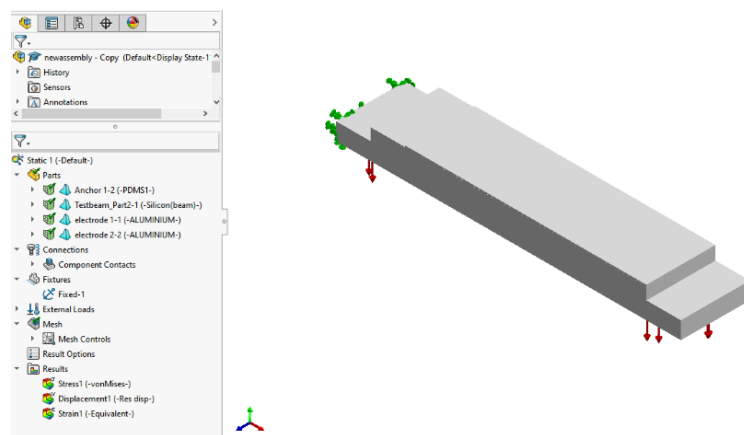


Figure 3-4 Stress analysis of the Sensor Model

In order to determine the strain value of the sensor attached beam, the static study was conducted by applying load (Pressure, Mpa) at the bottom layer of

cantilever beam. In this case, the strain value and maximum displacement of the beam were obtained as a result of simulation and they are important to show the impact of the applying load to the cantilever beam deflection. The data of the stress analysis is shown is table as below:

Table 3-2 Table of the displacement and strain

No.	Load/ 1×10^1 Mpa	Displacement /mm	Strain / $\mu\epsilon$
1	0	0	0
2	25	1.75E-02	7.27E-05
3	50	3.49E-02	1.45E-04
4	75	5.23E-02	2.18E-04
5	100	6.98E-02	2.91E-04
6	125	8.72E-02	3.63E-04
7	150	1.05E-01	4.36E-04
8	175	1.22E-01	5.09E-04
9	200	1.40E-01	5.81E-04
10	225	1.57E-01	6.54E-04
11	250	1.75E-01	7.27E-04
12	275	1.92E-01	7.99E-04
13	300	2.09E-01	8.72E-04
14	325	2.27E-01	9.45E-04
15	350	2.44E-01	1.02E-03
16	375	2.62E-01	1.09E-03

3.3.1(b) Stress Analysis: Create the deformed geometry of 2D sensor model

After obtaining magnitude of the distributed load that can generate the strain up to $1000\mu\epsilon$, 2D stress analysis was continued in the QuickField student 6.5. The 2D Sketching was located on x-y plane and it can be shown as figure below.



Figure 3-5 2D sketching of the sensor

Constraint boundary conQuickField student 6.5 has mesh limit at 255 degrees of freedom. This means that the model mesh couldn't be more than 255 nodes. The sensor model can be manually meshed by defining mesh spacing until get the maximum node number. Meshed model is shown as Figure 3-6.

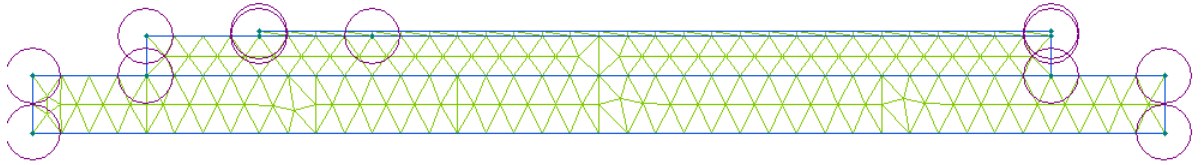


Figure 3-6 Meshed model.

StressDeform is a tool to convert the deformation result into a deformed geometry model (2D). This is important as the deformed geometry model will be used in the electrostatic analysis for simulating the capacitance output.



Figure 3-7 De-formed geometry of the sensor

3.3.2 Electrostatic Analysis: To obtain the capacitance output

QuickField Student 6.5 can perform linear electrostatic analysis for 2D models. Problem properties should be defined before the simulation. In this case, Plane parallel is chosen as the modal class since the sensor model will be simulated in right-handed Cartesian coordinate system. Other than that, the precision level can set to high level. Material properties, for an example, the dielectric constant of material will be defined and it is shown as below:

Table 3-3 Dielectric constant of the material

N0.1	Part	Material	Dielectric Constant
1.	Dielectric material and Anchor	PDMS	0.24
2.	Test Beam	Silicon	11.9
3.	Air gap	Air	1

Deformed 2D sensor model geometry was applied material at respective area that represents the sensor component. In this case, the boundary condition was set at the positive and negative conductive electrode. This is important to simulate the capacitance output of the sensor that is shown in figure below.